Journal of Siberian Federal University. Engineering & Technologies 2 (2009 2) 123-138
~ ~ ~

УДК 551.1

Trace-Element Analysis by Laser Ablation Inductively Coupled Plasma Mass Spectrometry (LA-ICP-MS): a Case Study for Agates from Nowy Kościoł, Poland

Robert Möckel[a], Jens Götze[a], Sergey A. Sergeev[b], Igor N. Kapitonov[b], Elena V. Adamskaya[b], Nikolay A. Goltsin[b] and Torsten Vennemann[c]*

[a] *TU Bergakademie Freiberg, Institute of Mineralogy, 14 Brennhausgasse, Freiberg, D-09596 Germany*

[b] *A.P. Karpinsky All Russian Geological Research Institute (VSEGEI), 74 Sredny Prospekt, St.-Petersburg, 199106 Russia*

[c] *Institut de Minéralogie et Géochimie, Université de Lausanne, UNIL-BFSH2, CH-1015 Lausanne, Switzerland* [1]

Received 6.05.2009, received in revised form 27.05.2009, accepted 17.06.2009

Laser ablation inductively coupled plasma mass spectrometry (LA-ICP-MS) was applied to detect trace elements in agate from Permian volcanics (Nowy Kościoł, Poland) in low concentrations and with high spatial resolution. The used LA-ICP-MS system consists of a DUV 193 laser ablation system linked to a Thermo Finnigan Element 2 mass spectrometer. The use of a 193 nm ArF excimer laser (50-200 mJ energy output) and the standards NIST 611 and NIST 612 enables to produce and analyse small crater diameters down to 5 μm.

Trace-element profiles have been analyzed for the elements Ti, Ge, Al, Fe, Mn, U, Th, Ba, Sr, Rb, Cs, and Y in the ppm- and sub-ppm level. The concentrations of the REE are sometimes below the detection limit of the method. Almost all elements (except Cu) display higher contents in chalcedony than in the macrocrystalline quartz. Fe, for instance, shows a 100 times higher concentration in agate bands compared to quartz, which may be due to finely distributed iron oxide particles in the chalcedony which probably act as colour pigments.

The trace elements in agate are released simultaneously with Si during alteration of the surrounding volcanic rocks. Oxygen isotope data indicate that silica accumulation and agate formation took place at temperatures below 120°C. The characteristic trace-element distribution patterns in agate result from a "self-purification" process during crystallization of chalcedony and quartz from a silica gel.

Keywords: agate, quartz, trace elements, LA-ICP-MS, oxygen isotopes, CL, Nowy Kościół.

1. Introduction

Agates are banded forms of microcrystalline α-quartz (chalcedony) and often form spectacular, multicoloured geodes or veins. These forms of SiO_2 can be found all over the world (Zenz 2005). Despite the intense research concerning the conditions of agate formation during the last 150 years,

* Corresponding author E-mail address: sazonov_am@mail.ru

detailed theories and suggestions are widespread and still controversely discussed (e.g., Godovikov et al. 1987; Blankenburg 1988). During the last decades, modern analytical methods such as fluid inclusion studies, oxygen isotope and traceelement analysis or luminescence microscopy and spectroscopy have been more involved into agate research (e.g., Blankenburg et al. 1982; Godovikov et al. 1987; Fallick et al. 1987; Harris 1988; Blankenburg et al. 1990; Strauch et al. 1994; Götze et al. 1999; Götze et al. 2001a; Moxon & Reed 2006). Nevertheless, many of the genetic problems are still unresolved and specific aspects have not been studied yet.

For instance, up to now only few information exist about the spatial distribution of trace elements in agates. Pilot studies by Heaney & Davis (1995) or Götze et al. (2001a) revealed that the trace element patterns of chalcedony and macrocrystalline quartz can be different in the same agate. On the other hand, rhythmic banding of agate layers can result in variations of the trace-element distribution. The detailed knowledge about the trace-element behaviour may provide further information about the physico-chemical conditions during agate formation.

The method of laser ablation inductively coupled plasma mass spectroscopy (LA-ICPMS) is available since the mid-1980s (Gray 1985) and seems to suit perfectly to determine a spatial resolved trace-element distribution in agates. During the last two decades, the method was brought to perfection with detection limits down to a few ppb, depending on analytical conditions (e.g. spot size) and sample material (Günther 2001). Recently, LA-ICP-MS is a widely accepted powerful analytical method in science and technology, including geoscientific research. An overview about requirements and recent technical developments is given in Flem et al. (2002), Heinrich et al. (2003) or Günther & Hattendorf (2005). In the present study, LA-ICP-MS was firstly applied to the study of agate to answer the questions: (1) is LA-ICP-MS applicable for very low trace-element contents expected in quartz (agate), and (2) is it possible to detect trace-element variations with high spatial resolution along a profile perpendicular to the agate banding.

2. Materials and Methods

The agate material investigated in the present study originates from occurrences in the vicinity of Nowy Kościół (Lower Silesia, Poland). The agate outcrops occur at the bottom part of Permian rhyolites and rhyodacites close to the contact with Middle Rotliegend tuffs and Upper Permian claystones (Gaweda and Rzymełka 1992). Porphyric nodules are mostly spherical shaped and can reach sizes of 2–70 cm in diameter. The agates from Nowy Kościoł show both chalcedony bandings and macrocrystalline quartz zones. They are typically multicoloured fortification agates with shades of white, reddish, green, brown and yellow (Fig. 1). Several accessoric phases have been detected in the agates including hematite, sulphide minerals and monazite (Gaweda and Rzymełka 1992, Dumańska-Słowik et al. 2008). A specific feature is the occurrence of organic matter (aliphatic and subordinately aromatic compounds), which has been related to the postgenetic alteration of the volcanic rocks (Dumańska-Słowik et al. 2008).

The phase composition of the volcanic host rocks was determined by X-ray diffraction (XRD) studies. Therefore, material from the surrounding adjacent host rock of the agates was separated and grinded to <20 μm grain size. An URD 6 XRD device (Seifert/Freiberger Präzisionsmechanik) with CoKα radiation was used and the irradiated area was kept constant at 15 mm^2. Samples were scanned with 2θ-steps of 0.03° in the range from 5–80° at step times of 5 seconds per step.

Quantification of powder diffraction patterns was carried out using the Rietveld algorithm BGMN (Taut et al. 1998).

Polished thin sections of agates and surrounding host rocks were prepared for microscopic studies (ZEISS Axio Imager A1m) to get information about internal agate structures. In addition, CL measurements on carbon coated thin sections were performed using a "hot cathode" CL microscope HC1-LM (Neuser et al. 1995). The system was operated at 14 kV accelerating voltage and a current density of about 10 μA/mm^2. Luminescence images were captured "on-line" during CL operations using a peltier cooled digital videocamera (KAPPA 961-1138 CF 20 DXC). CL spectra in the wavelength range 380 to 900 nm were recorded with an Acton Research SP-2356 digital triple-grating spectrograph with a Princeton Spec-10 CCD detector that was attached to the CL microscope by a silica-glass fibre guide.

Oxygen isotopic studies on macrocrystalline quartz and chalcedony were performed by a microanalytical laser-based method at the University of Lausanne, Switzerland. Small samples free of visible microinclusions were placed on a nickel sample holder and were heated with a 20 W CO_2 laser, while fluorinating due to BrF_5 atmosphere. The released oxygen was converted to CO_2 by combustion with a hot carbon rod after passing over a cold trap and through a hot mercury fluorine-getter and then admitted on-line to the mass spectrometer. The precision and accuracy of the method is ± 0.1 ‰ for < 100 μg samples (Sharp 1992).

For trace-element analysis by LA-ICP-MS, a section perpendicular to the agate banding was cut, polished and fixed with epoxy resin in a 1 inch diameter ring, which fits in the sampling cell of the LA-ICP-MS device (see marked area in Fig. 2). Measurements were performed at the VSEGEI (St. Petersburg, Russia) on a system with a *Thermo Finnigan Element 2* mass spectrometer, linked to a *DUV 193* laser ablation system including optics and viewing by *New Wave Research/Merchantek Products*. A principle sketch of a LA-ICP-MS system is given in Fig. 3. The ArF excimer laser operates with a wavelength of 193 nm and an energy output of 50–200 mJ. This constellation enables to produce and analyse small craterdiameters down to 5 μm. The two accredited standards NIST 611 and NIST 612 were used for calibration procedures (Hollocher & Ruiz, 1995). Calibration procedures were made at the beginning and at the end of the measuring cycle and after analysing five spots, mainly in order to minimize memory effects. The parameters of the system are given in Table 1.

Trace elements were classified concerning possible overlapping of their mass/charge ratio and first measured with low resolution (LR, R=300) and medium resolution mode (MR, R=4000), respectively. Table 2 shows the modes for the measured isotopes. Isotopes were selected considering natural abundances. However, the higher resolution mode is opposite to intensity and therefore, to the detection limit, which is around 0.01 ppm and 1 ppm for LR and MR, respectively. The given values are approximate values, since the detection limit is typically three times the standard deviation of the noise level (blank). Strictly speaking, the detection limit has to be calculated for each element and analyzing spot, resulting in varying detection limits depending on the specific trace element concentration. Because of this limitation, the approximate values as stated above were set after all measurements and proved to be adequate. The same strategy was applied for the error of measurements, which is estimated to be below 5–10% for all values given below. In order to lower the analytical error, the measurements of all elements was repeated 20 times on each spot.

As can be seen in Fig. 4, a typical signal of LA-ICP-MS measurement for a single element during ablation of material consists of three phases. In the first phase, the blank from the carrier gas

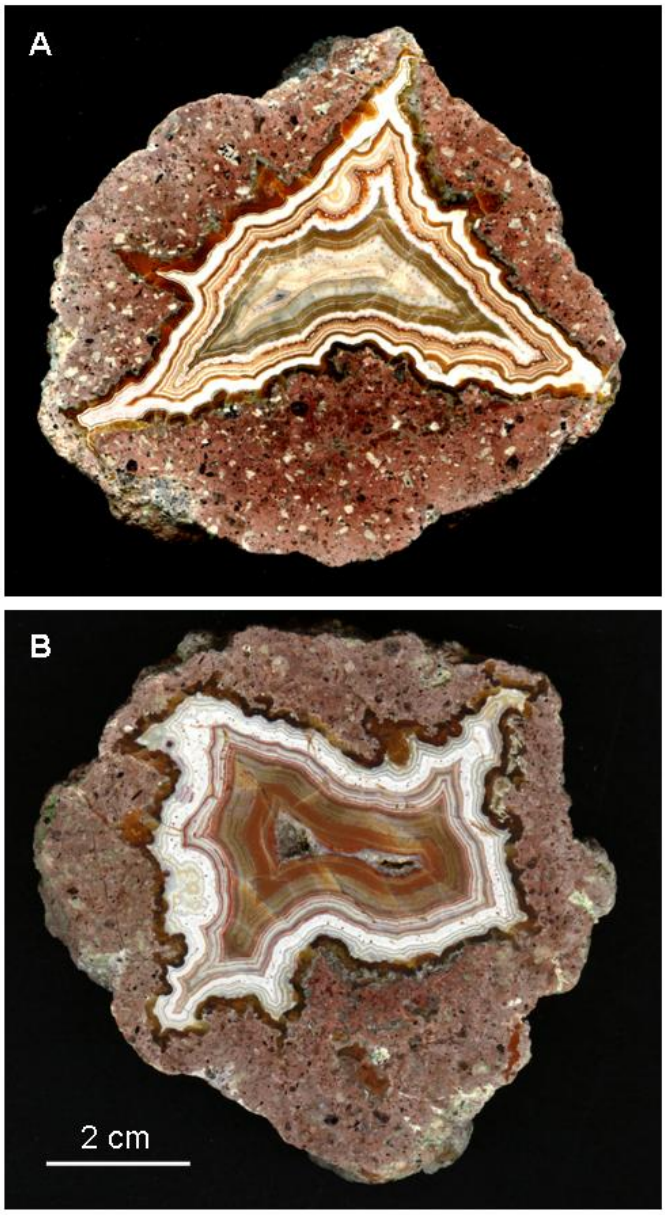

Fig. 1. Multi-coloured volcanic agates from Novy Kościół (Poland) with typical fortification banding

Fig. 2. Selected agate from Novy Kościół (Poland) for detailed LA-ICP-MS investigations; the rectangle represents the prepared area for the trace-element profile

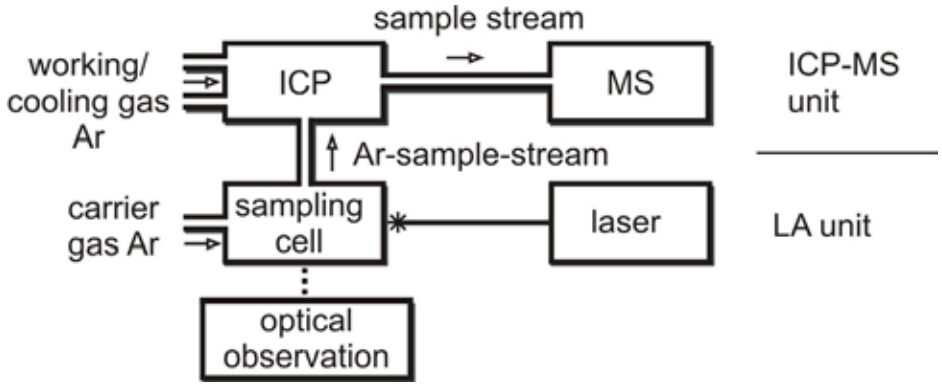

Fig. 3. Schematic sketch of the LA-ICP-MS device

Table 1. Technical parameters of the LA ICP-MS system

Excimer Laser Compex	
Energy output	50–200 mJ
pulse duration/repetition frequency	15 ns/ 1–20 Hz
beam diameter	5–300 µm
carrier	gas
Thermo Finnigan Element 2	
type	sector field mass spectrometer
auxiliary gas flow	approx. 1 l/min (optimized automatically)
cooling gas flow	approx. 15 l/min (optimized automatically)
power	approx. 1 kW

Table 2. Selected isotopes for LA-ICP-MS measurements (LR low resolution mode, MR medium resolution mode). Distributions of trace elements printed in bold letters are displayed in Fig. 7 and 8.

LR	**^{7}Li, ^{27}Al,** ^{28}Si, ^{29}Si, ^{44}Ca, ^{60}Ni, **^{69}Ga, ^{71}Ga**, **^{72}Ge, ^{74}Ge, ^{85}Rb, ^{88}Sr,** ^{89}Y, **^{133}Cs**, **^{138}Ba,** ^{139}La, ^{140}Ce, ^{141}Pr, ^{142}Nd, ^{146}Nd, ^{147}Sm, ^{151}Eu, ^{153}Eu, ^{155}Gd, ^{157}Gd, ^{159}Tb, ^{161}Dy, ^{163}Dy, ^{165}Ho, ^{166}Er, ^{167}Er, ^{169}Tm, ^{172}Yb, ^{173}Yb, ^{175}Lu, ^{232}Th, **^{238}U**
MR	**Na^{12}**, ^{29}Si, ^{30}Si, ^{47}Ti, ^{55}Mn, **^{56}Fe, ^{57}Fe,** ^{59}Co, ^{60}Ni, ^{62}Ni, **^{63}Cu, ^{65}Cu**

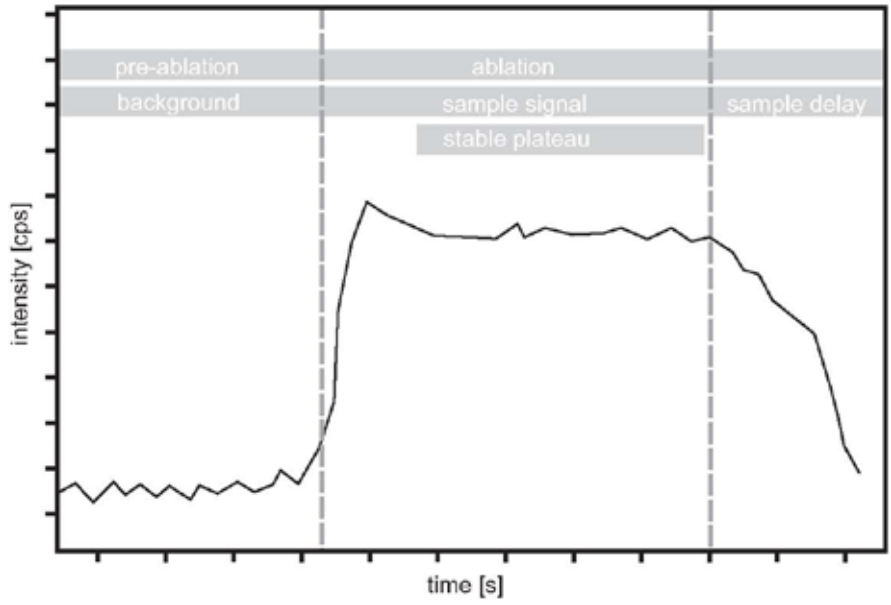

Fig. 4. A simplified diagram of a typical LA-ICP-MS signal for one element displaying three different phases

is recorded, where no laser action takes place and no sample material is introduced into the ICP-MS. The initiation of the laser is marked by rapid increase of the signal, followed by a stable plateau phase during which sample material is constantly carried to the ICP-MS (phase two). The proper value of intensity is averaged from this stable plateau. Of course the length of this plateau depends on the volume of ablated material and therefore, on laser parameters (laser pulse, repetition rate etc.) and not least on the material. Phase three is characterized by a steady decrease of the intensity down to the blank level, after ablation ended.

Measuring points were chosen to be located in both agate and macrocrystaline quartz areas, with an average distance of 870µm. Since the amount of ablated material from one "shot" is insufficient for operating 20 analyses, there had to be done several "laser shots" arranged in a row in order to avoid fractionating processes in the crater (Fryer et al. 1995; Günther & Hattendorf 2005; Fernández et al. 2007).

3. Results and discussion

Agate formation and structure

The XRD analyses provided first results concerning the mineral composition of the adjacent host rocks of the agates (Table 3). The fresh material is dominated by quartz and K-feldspar and represents a rhyolitic composition. Alteration processes resulted in a loss of amorphous material (glassy matrix) and feldspar, respectively and the formation of clay minerals (especially illite). The illitization of the volcanic host rocks can be one of the processes providing silica for the agate formation.

For the estimation of formation temperatures, $\delta^{18}O$ values were measured for the silica matrix. The $\delta^{18}O_{SMOW}$ data of the analyzed agate range from 29.36 ‰ (quartz) to 30.25 ‰ (chalcedony) (Table 4). Because of the unknown origin of the participating fluids, the temperatures were calculated for different sources according to Méheut et al. (2007) (see Table 4). The calculations point to relatively low temperatures between 20°C and 120°C. These results are in accordance with measured homogenization

Table 3. Phase composition of adjacent host rocks of the investigated agates determines by XRD analysis (contents in weight-%)

	Fresh host rock (greyish brown)	Altered host rock (greenish)
Quartz	35 ± 2	35 ± 1
Monoclinic K-feldspar	40 ± 2	38 ± 2
Plagioclase	6 ± 1	5 ± 1
Kaolinite	2 ± 1	4 ± 1
Illite	2 ± 1	9 ± 1
Amorphous	15 ± 4	10 ± 3

Table 4. Oxygen isotope data of agate and quartz with calculated temperatures according to Méheut et al. (2007); the temperatures are calculated for fractionation with meteoric water (-10‰), oceanic water (±0‰) and magmatic water (+8‰)

Sample	$\delta^{18}O_{SMOW}$(‰)	T_{met} (°C)	T_{oc} (°C)	T_{mag} (°C)
quartz	29.36	31	70	115
agate	30.25	28	66	109

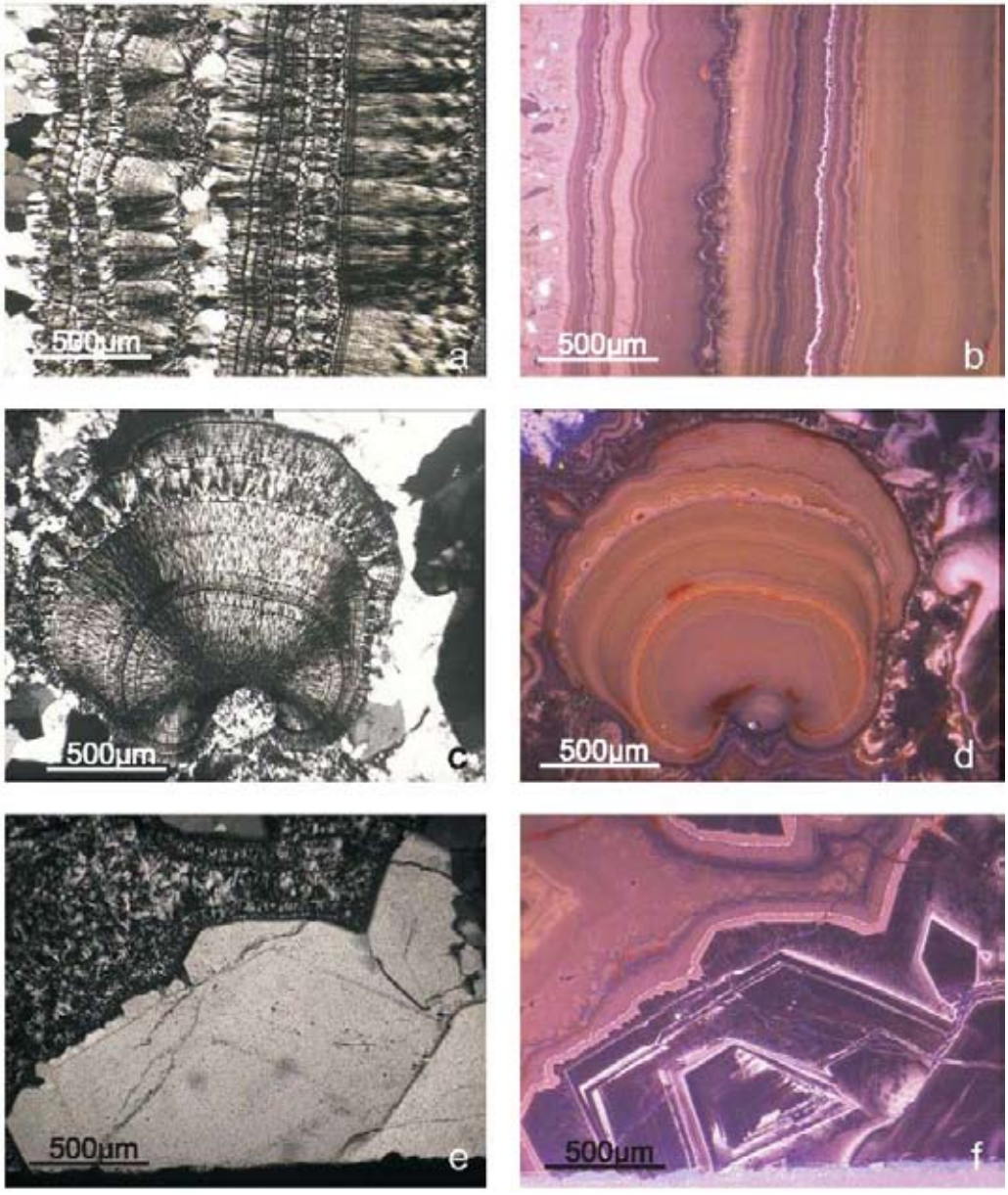

Fig. 5. Polarized light (Pol) and cathodoluminescence (CL) micrograph pairs of the investigated agates from Novy Kościół (Poland); (a) alternate bedding of chalcedony bands and macrocrystalline quartz layers showing varying CL colours; (b) spherulitic chalcedony growth with distinct internal structure; (c) strongly zoned macrocrystalline quartz

temperatures of primary fluid inclusions in quartz, which scatter between 100 and 215°C (Kozłowski 1985).

The agates itself are typically banded with alternate bedding of chalcedony bands and macrocrystalline quartz layers (Fig. 5a). Isolated spherulitic silica growth is common (Fig. 5b), and areas with macrocrystalline quartz have formed in the central and marginal parts of the agates (Fig. 5c). In some cases, the transition from quartz to chalcedony is sharp. Iron oxides are often interbedded

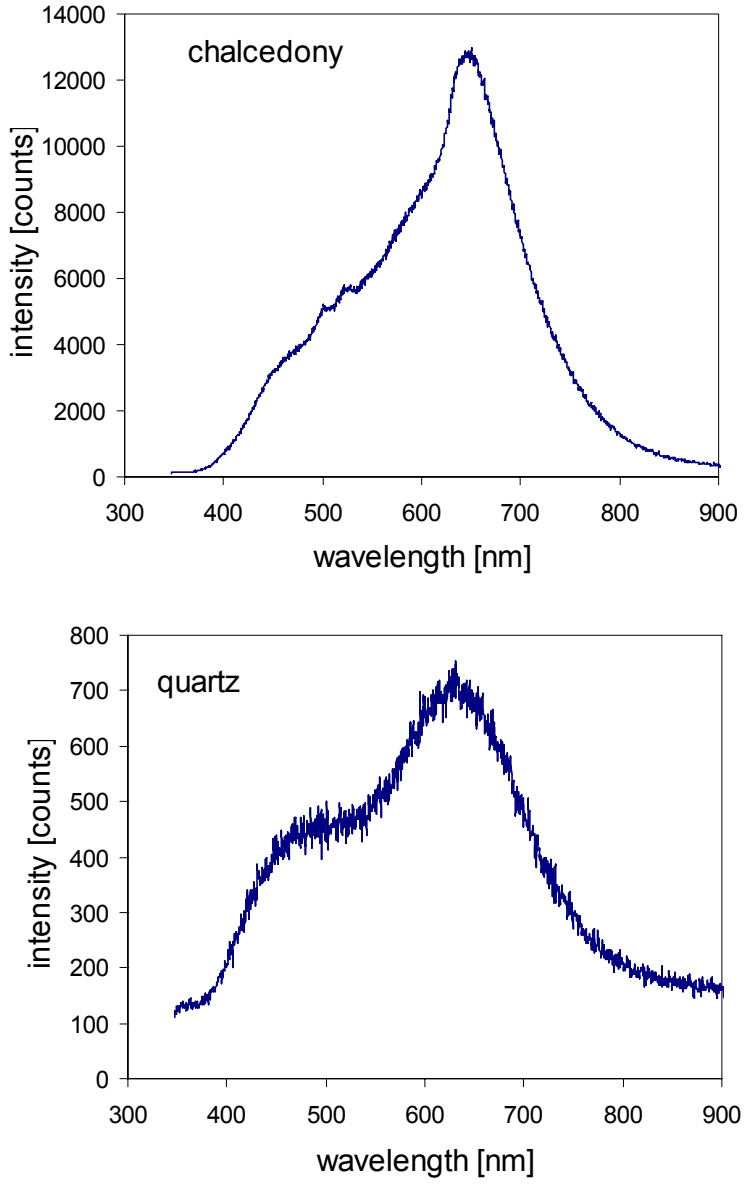

Fig. 6. Typical CL spectra from chalcedony and macrocrystalline quartz; the CL spectrum of quartz shows two broad emission bands at 450-500 nm and ca. 650 nm; the CL of chalcedony is dominated by a strong emission band at 650 nm and shows at least three additional bands (shoulders) at 580, 500 and 450 nm

along the crystallization front of chalcedony, probably resulting from a "self-purification" process of originally iron-rich silica.

CL imaging revealed several differently coloured zones within the agates. The chalcedony layers display reddish, rose and orange colours (Fig. 5). Phanerocrystalline quartz may exhibit similar CL colours as the surrounding chalcedony, but sometimes more bluish CL colours and distinct complex zoning (both sector and concentric zoning) (Fig. 5). The comparison of the differently luminescent agate bands and macrocrystalline quartz (Fig. 6) illustrates that the CL spectra generally consist of the same emission bands. The different CL colours and intensities, respectively, are a result of

varying intensity ratios of the main CL emission bands. The most common and most intense CL emission band occurs around 650 nm (Fig. 6) and is related to the so called non-bridging oxygen hole centre (NBOHC; Siegel and Marrone 1981). This defect type may result from several precursors such as silanol groups, peroxy linkage (oxygen-rich samples) or strained Si-O bonds (Stevens Kalceff et al. 2000). In the case of agates we have high contents of silanol groups (Si-OH), which are common in microcrystalline quartz (Flörke et al. 1982; Götze et al. 1999; Moxon and Reed 2006). The lower intensity of the 650 nm emission in macrocrystalline quartz is a result of the lower density of this defect type.

Other emission bands (450 nm, 580 nm) appear only subordinately, partly as shoulder of the main CL emission (Fig. 6). The yellow CL emission (580 nm), which can be related to the E' centre (electron defect on an oxygen vacancy), was up to now only observed in agates, silicified wood and hydrothermal quartz (Götze et al., 1999, 2001b; Moxon and Reed 2006). The emission band around 450 nm, which is especially present in macrocrystalline quartz, is due to the recombination of the so-called self-trapped exciton (Stevens Kalceff et al. 2000), an electron hole pair on an oxygen vacancy and a peroxy linkage. The oxygen vacancies may indicate crystallization under conditions with oxygen deficit.

The results of the microscopic studies indicate that the agate crystallized in a continuous process from a silica-rich precursor. Crystallization started with spherulitic growth and the formation of chalcedonic quartz, later changing into well developed crystals. Accordingly, the phanerocrystalline quartz seems to be the prosecution of chalcedony "fibres". The high defect density and the occurrence of sector zoning in quartz may result from rapid crystallization under non-equilibrium conditions. Except for the outermost layer of chalcedony, CL colours and spectra are almost the same in both quartz and chalcedony and display a similar local defect structure, which implies the origin from a single ongoing crystallization process. The sometimes observed repeated change between chalcedony and macrocrystalline quartz layers may result from changes in the silica concentration of the mineralizing fluids or from several mineralization stages.

Trace element studies by LA-ICP-MS

The results of the present study show that most of the measured trace-elements are present in very low concentrations. Because of the specific analytical conditions, the limits of detection vary for different elements (Table 5). Therefore, the strategy of the analytical procedure was to lower the limits of detection by repeated "laser shots" (more sample material) and valuable standard materials. Nevertheless, concentrations of some elements were below the detection limits. For example, the contents of the rare earth elements (REE) did not provide important data in terms of REE distribution patterns.

Problems during measurements appeared with Ca and Ni. Ni is part of the cone material of the skimmer technology of the mass spectrometer. Ni was measured in LR as well as MR mode (see Table 2), mostly in order to avoid overlapping with other isotopes (e.g. $^{44}Ca^{16}O$, $^{24}Mg^{36}Ar$). However, measured values differed sometimes more than 50% and therefore, have been not reliable. The ^{44}Ca values were mostly unreliable as well due to overlapping with $^{28}Si^{16}O$, which is basic matrix material. A higher resolution mode for Ca or the use of another inert gas instead of argon (^{40}Ar overlaps ^{40}Ca), respectively, may prevent this problem. In the present study, the problem was tried to solve by an afterwards calculation of a $^{28}Si^{16}O$-blank. Although the measured Ca contents are similar to

Table 5. Average trace-element contents and variation limits (in ppm) of the investigated profile perpendiculat to the agate banding (see Fig. 2) (quartz: measunring points 1–7; agate: measuring points 8–12)

	quartz			agate		
	average	**max**	**min**	**average**	**max**	**min**
Li	1.01	2.77	0.03	2.73	4.69	0.84
Na	24.0	59.2	1.35	192.3	294.1	106.7
Al	13.7	47.2	2.71	325.4	640.8	58.0
Ge	0.63	1.06	0.32	12.12	20.42	7.42
Rb	0.12	0.17	0.07	1.60	3.05	0.66
Sr	0.07	0.09	0.03	3.29	7.58	0.48
Ba	1.40	0.37	0.03	5.00	6.38	0.19
Y	0.01	0.02	0.01	0.20	0.62	0.03
La	0.09	0.09	0.08	–	–	–
Ce	0.10	0.12	0.08	0.04	0.12	0.01
Nd	0.03	0.03	0.03	0.05	0.05	0.05
Sm	0.02	0.02	0.01	–	–	–
Eu	–	–	–	0.01	0.01	0.01
Gd	–	–	–	0.03	0.04	0.01
Dy	–	–	–	0.04	0.08	0.01
Ho	–	–	–	0.03	0.03	0.03
Er	–	–	–	0.03	0.04	0.01
Tm	–	–	–	0.01	0.01	0.01
Yb	–	–	–	0.06	0.06	0.06
Th	0.37	0.37	0.37	0.02	0.03	0.01
U	0.15	0.02	0.52	2.39	3.37	1.81
Ti	<1	<1	<1	1.20	3.40	<1
Mn	<1	<1	<1	0.61	1.39	<1
Fe	0.95	2.62	<1	90.4	119.8	69.3

(-) below detection limit

concentrations (330–634 ppm) reported by Dumańska-Słowik et al. (2008), there was still some doubt on the reliability of these corrected values and therefore, they will not be presented here.

A number of trace-elements could be analyzed with high precision. The results of the trace-element analyses are given in Table 5 (average values and limits of variation). The spatial distribution of selected element contents is presented in Fig. 7 and 8. The comparison of the data from Nowy Kościół with trace element contents of agates from different regions (e.g., Blankenburg 1988, Götze et al. 2001) revealed that concentrations presented here are slightly below other published values, but more or less in the same order of magnitude. In general, it is obvious that a number of elements is accumulated in agate. Besides the common elements Al, Fe, and Na, also Ba, Sr, U and Ge show relatively high concentrations. These elements may be mobilized together with Si during the alteration of the volcanic host rocks. The decomposition of volcanic glass and feldspar provides high amounts of Si, Al, Ca, Na and K. The mobility of U during the alteration of volcanic rocks was reported by Zielinski (1979) who observed the parallel accumulation of Si and U. In the case of Ge, the identical geochemical character

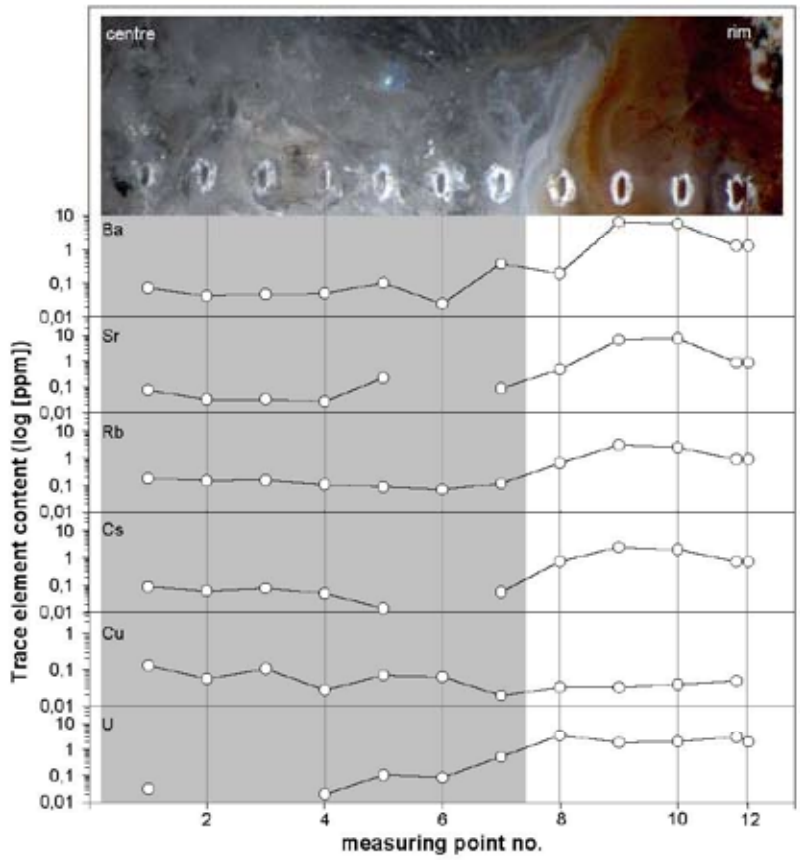

Fig. 7. Distribution profiles of selected trace elements (Ba, Sr, Rb, Cs, Cu, U) in the investigated agate from Novy Kościół (Poland)

with Si promotes the common transport and the incorporation of Ge into the quartz structure (e.g., Walenzak 1969, Götze et al. 2004). Therefore, high concentrations of Ge are typical for agates from acidic host rocks (Blankenburg 1988).

One characteristic feature of the trace-element distributions is that almost all elements show higher contents in chalcedony compared to macrocrystalline quartz (Fig. 7 and 8). Aluminium, for instance, has an average concentration of 325.4 ppm in chalcedony and 13.7 ppm in quartz. Fe shows a hundred times higher concentration in chalcedony parts (average 90.4 ppm) than in the quartz centre (average 0.95 ppm). The only exception for this is Cu, which is slightly enriched in quartz (average of 0.07 ppm) compared to chalcedony (average 0.04 ppm). Moreover, elements which behave geochemically similar such as Ba and Sr or Rb and Cs display comparable patterns (Fig. 7). These similar patterns suggest a simultaneous mobilization and precipitation of the elements.

The differences in most element concentrations between chalcedony and quartz can probably be explained by a "self-purification" process during the crystallization of the agate. The trace elements are firstly precipitated together with the primary silica gel and are finely dispersed in the silica matrix. Starting spherulitic growth of the chalcedony may initially incorporate high contents of trace elements. During further growth, the concentration of impurities drops, which is macroscopically detectable in the changing visible colour of the agate bands. In general, deeply coloured parts of the agate inherit

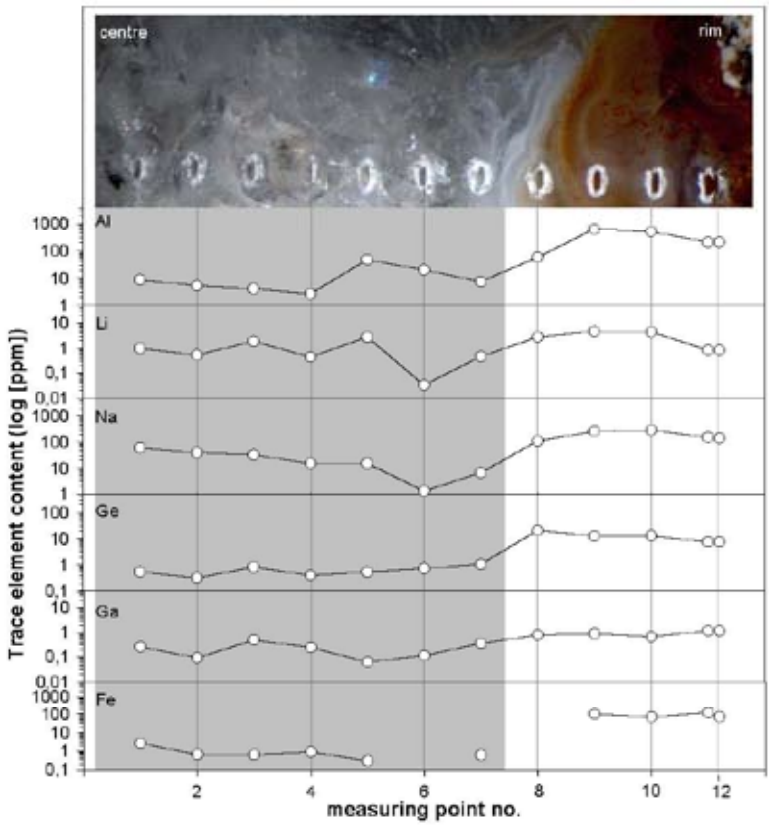

Fig. 8. Distribution profile of selected trace elements (Al, Li, Na, Ge, Ga, Fe) in the investigated agate from Novy Kościół (Poland)

higher trace-element concentrations than colourless parts. For example, the outermost measuring points are situated in a dark reddish band and reveal in almost all cases higher element contents, whereas the colour gets more and more light towards the inner core.

Heaney (1993) stated that the high trace-element contents in silica can cause the formation of frequent defects, Brazil twinning and typical twisting in chalcedony. He concluded that chalcedony fibres in agates may be the result of dislocation growth. This statement would explain why macrocrystalline quartz can only grow after removing most of the impurities. The transition zone between chalcedony and quartz is characterized by a characteristic drop of most trace-element contents. On the other hand, the higher defect density in chalcedony was also detected by CL spectroscopy.

The kind of incorporation of various trace elements into quartz can be different (Götze et al. 2004). Whereas Al, Ti, Ge, Fe, Na or Li are often substitute for Si or placed at interstitial lattice positions, elements such as Ba, Sr, Rb, Cs or U may be concentrated in fluid and mineral inclusions or at grain boundaries. However, the incorporation into the quartz structure is limited as is visible for iron. The occurrence of high iron contents and sometimes iron oxides within the agate matrix is an indication for high iron contents of the silica-bearing mineralizing medium. The accumulation of hematite spheres along the banding of the next chalcedony layers may be a result of the "self-purification" of chalcedony during crystallization. The iron was removed from the silica during crystallization, moved with the

crystallization front and accumulated forming iron oxide spheres. Especially the coloured agate bands exhibit high concentrations of iron emphasizing that iron is mostly concentrated in fine iron oxide particles within the chalcedony layers acting as colour pigments.

4. Conclusions

The results of the present study clearly demonstrate that LA-ICP-MS is a suitable analytical method for the detection of trace elements in very low concentrations. Although the element contents of most of the elements in quartz are in the ppm and sub-ppm level, the method enables to realize a spatially resolved analysis. Therefore, the method provides valuable data for genetic interpretations in samples with marked micro- and/or macro-textures. Only for a few elements (especially the REE), the concentrations are often too low to be detected by LAICP-MS.

The trace-element analysis with high spatial resolution enabled to monitor the distribution of specific elements during proceeding agate formation. One characteristic feature is the release of elements (e.g., Al, Fe, Ge) together with Si from the volcanic host rocks due to the ongoing alteration, and the subsequent accumulation within the silica matrix during agate formation. Elements showing a similar geochemical behaviour (e.g., Ba-Sr or Rb-Cs) display identical spatial distribution pattern within the agate texture. Most of the impurities precipitate at the beginning of the agate formation, whereas further growth and crystallization of the silica matrix results in lower impurity concentrations. Within the last-stage macrocrystalline quartz in the agate centre, trace-element contents are very low or even not detectable. These facts point to a "self-purification" process of the silica matrix during ongoing crystallization, sometimes resulting in the admixture of impurity phases (e.g. iron oxides/-hydroxides).

Acknowledgement*: We gratefully acknowledge providing of agate samples from Novy Kościół by Marek Stepisiewicz (Warsaw). We also thank Dmitry Sergeev for helping a lot to overcome language barriers at the VSEGEI St. Petersburg.*

References

Blankenburg, H.-J., Pilot, J., Werner, C.D. (1982) Erste Ergebnisse der Sauerstoffisotopenuntersuchungen an Vulkanitachaten und ihre genetische Interpretation. Chemie Erde 41: 213–217.

Blankenburg, H.-J. (1988) Agate. VEB deutscher Verlag für Grundstoffindustrie, Leipzig (in German)

Blankenburg, H.-J., Thomas, R., Klemm, W., Leeder, O. (1990) Interpretation der Ergebnisse von Einschlußuntersuchungen an den Quarzinkrustaten aus Vulkanitachaten. Zeitschrift für geologische Wissenschaften 18: 81–85.

Dumańska-Słowik, M., Natkaniec-Nowak, L., Kotarba, M.J., Sikorska, M., Rzymetka, J.A., Loboda, A., Gaweł, A. (2008) Mineralogical and geochemical characterization of the "bituminous" agates from Nowy Kościół (Lower Silesia, Poland). Neues Jahrbuch für Mineralogie, Abhandlungen 184(3): 255–268.

Fallick, A. E., Jocelyn, J., Donnelly, T., Guy, M., Behan, C. (1985) Origin of agates in volcanic rocks from Scotland. Nature 313: 672–674.

Fallick, A. E., Jocelyn, J., Hamilton, P. J. (1987) Oxygen and Hydrogen stable isotope systematics in brazilian agates. In: Rodriguez-Clemente, R. and Tardy, Y. (Eds.), Geochemistry and mineral formation in the earth surface, 99–117.

Fernández, B., Claverie, F., Pécheyran, C., Donard, O. (2007) Direct analysis of solid samples by fs-LA-ICP-MS. Trends in Analytical Chemistry 26(10): 951–966.

Flem, B., Larsen, R.B., Gromstvedt, A., Mansfeld, J. (2002) In situ analysis of trace elements in quartz by using laser ablation inductively coupled plasma mass spectrometry. Chemical Geology 182: 237-247.

Flörke, O.W., Köhler-Herbertz, B., Langer, K., Tönges, I. (1982) Water in microcrystalline quartz of volcanic origin: agates. Contributions to Mineralogy and Petrology, 80, 324-333.

Fryer, B.J., Jackson, S.E., Longerich, H.P. (1995) The design, operation and role of the laserablation microprobe coupled with an inductively coupled plasma-mass spectrometer (LAM-ICP-MS) in the earth sciences. The Canadian Mineralogist 33: 303–312

Gaweda, A. and Rzymełka, J.A. (1992) Bituminous agates from rhyolites in the environs of Nowy Kościół, Lower Silesia. Mineralogia Polonic 23(1): 72–84

Godovikov, A.A., Ripinen, I.I., Motorin, S.G. (1987) Agates. Izd. Nedra, Moscow (in Russian).

Götze, J., Plötze, M., Fuchs, H., Habermann, D. (1999) Defect structure and luminescence behaviour of agate - results of electron paramagnetic resonance (EPR) and cathodoluminescence (CL) studies. Mineralogical Magazine 63: 149-163.

Götze, J., Tichomirowa, M., Fuchs, H., Pilot, J., Sharp, Z.D. (2001a) Geochemistry of agates: a trace element and stable isotope study. Chemical Geology 175: 523–541.

Götze, J., Plötze, M., Habermann, D. (2001b) Origin, spectral characteristics and practical applications of the cathodoluminescence (CL) of quartz – a review. Mineralogy and Petrology 71: 225–250.

Götze, J., Plötze, M., Graupner, T., Hallbauer, D.K., Bray, C. (2004) Trace element incorporation into quartz: a combined study by ICP-MS, electron spin resonance, cathodoluminescence, capillary ion analysis and gas chromatography. Geochimica et Cosmochimica Acta 68: 3741-3759.

Günther, D. and Hattendorf (2005) Solid sample analysis using laser ablation inductively coupled plasma mass spectrometry. Trends in Analytical Chemistry 24(3): 255–265

Gray, A.L. (1985) Solid sample introduction by laser ablation for inductively coupled plasma source mass spectroscopy. Analyst 110: 551–556

Heaney, P. J. (1993) A proposed mechanism for the growth of chalcedony. Contributions to Mineralogy and Petrology 115: 66 – 74.

Heaney, P. J. & Davis, A. M. (1995) Observation and origin of self-organized textures in agates. Science 269: 1562 – 1565.

Harris, C. (1988) Oxygen isotope Geochemistry of a Quartz-Agate Geode from northwestern Namibia. Communs geol. Surv. S.W. Africa Namibia 4: 43–44.

Heinrich, C.A., Pettke, T. Halter, W.E. Aigner-Torres, M., Audétat, A., Günther, D., Hattendorf, B., Bleiner, D., Guillong, M., Horn, I. (2003) Quantitative multi-element analysis of minerals, fluid and melt inclusions by laser-ablation inductively-coupledplasma mass-spectrometry. Geochimica et Cosmochimica Acta 67(18): 3473–3496

Hollocher and Ruiz (1995) Major and trace element determinations on NIST glass standard reference materials 611, 612, 614 and 1834 by inductively coupled plasma-mass spectrometry. Geostandards Newsletter 19(1): 27–34

Kozłowski, A. (1985) Studies of fluid inclusions in agates from Plóczki Górne and Nowy Kościół, Poland. Fluid Inclusion Research – Proceedings of COFFI, Michigan University Press, Ann Arbor, USA, 18: 221-222.

Méheut, M., Lazzeri, M., Balan, E., Mauri, F. (2007) Equilibrium isotopic fractionation in the kaolinite, quartz, water system: Prediction from first-principles density-functional theory. Geochimica et Cosmochimica Acta 71: 3170–3181.

Moxon, T. and Reed, S.J.B. (2006) Agate and chalcedony from igneous and sedimentary hosts aged from 13 to 3480 Ma: a cathodoluminescence study. Mineralogical Magazine 70: 485–498

Möckel, R. and Götze, J. (2007) Agates from volcanics of the Erzgebirge Basin, Saxony (in German). Veröffentlichungen des Museums für Naturkunde Chemnitz 30: 25-60.

Neuser, R.D., Bruhn, F., Götze, J., Habermann, D., Richter, D.K. (1995) Kathodolumineszenz: Methodik und Anwendung. Zentralblatt für Geologie und Paläontologie, Teil I, H. 1/2: 287-306.

Sharp, Z.D. (1992) In situ laser microprobe techniques for stable isotope analysis. Chemical Geology 101: 3-19.

Siegel, G. H. and Marrone, M. J. (1981) Photoluminescence in as-drawn and irradiated silica optical fibers: An assessment of the role of nonbridging oxygen defect centres. Journal of Noncrystalline Solids 45: 235–247.

Stevens Kalceff, M.A., Phillips, M.R., Moon, A.R., Kalceff, W. (2000) Cathodoluminescence microcharacterisation of silicon dioxide polymorphs. In: Pagel, M., Barbin, V., Blanc, P., Ohnenstetter, D. (eds.) (2000) Cathodoluminescence in geosciences. Springer Verlag, Berlin Heidelberg New York, 193-224.

Strauch, G., Nitzsche, H.-M., Holzhey, G. (1994) Isotopenuntersuchungen an Rhyolithen und Achatbildungen. N. Jb. Mineral., Abh. 165: 103–104.

Taut, T., Kleeberg, R., Bergmann, J. (1998) Seifert Software: The new Seifert Rietveld program BGMN and its application to quantitative phase analysis. Materials Structure 5(1): 57–66.

Walenzak, Z. (1969) Geochemistry of minor elements dispersed in quartz (Ge, Al, Ga, Fe, Ti, Li and Be). Archiwum Mineralogiezne 28: 189-335.

Zenz, J. (2005) Agate. Bode Verlag, Haltern.

Zielinski, R.A. (1979) Uranium mobility during interaction of rhyolitic obsidian, perlite and felsite with alkaline carbonate solution: T=120°C, P=210 kg/cm^2. Chemical Geology 27: 47-63.